Green Chemical Technology

SCIEPublish

Article

Investigation into the Role of Recycled Coarse Aggregate Quality in the Behavior of Geopolymer Recycled Pervious Concrete

Meirong Zong [1], Yuting Sun [1], Xinyu Liu [2], Hui Liu [1,*], Pinghua Zhu [1] and Faqin Dong [3]

[1] Department of Civil Engineering, Changzhou University, Changzhou 213164, China; meirongzongslp@cczu.edu.cn (M.Z.); s24210814016@smail.cczu.edu.cn (Y.S.); zph@cczu.edu.cn (P.Z.)

[2] Myande Group Co., Ltd., Yangzhou 225127, China; liuxinyu@myande.com (X.L.)

[3] Key Laboratory of Waste Solid Treatment and Resource Recycle of Ministry of Education, Mianyang 621010, China; fqdong@swust.edu.cn (F.D.)

* Corresponding author. E-mail: liuhui@cczu.edu.cn (H.L.)

Received: 24 January 2026; Revised: 2 April 2026; Accepted: 29 April 2026; Available online: 14 May 2026

ABSTRACT: Geopolymer recycled pervious concrete (GRPC) provides a promising solution for low-carbon construction through the utilization of industrial by-products and recycled coarse aggregates (RCA). However, the influence of RCA quality on the durability performance of GRPC remains insufficiently understood. In this study, GRPC was prepared using RCA of high, medium, and low quality, denoted as H-GRPC, M-GRPC, and L-GRPC, respectively. The mechanical properties, permeability, fatigue resistance, freeze-thaw resistance, and microstructural characteristics were systematically investigated. The results showed that RCA quality had a limited effect on permeability, whereas the mechanical performance and durability of GRPC were strongly dependent on RCA quality. The initial compressive strengths of H-GRPC, M-GRPC, and L-GRPC were 79.2, 75.3, and 60.0 MPa, respectively, with corresponding flexural strengths of 7.3, 6.7, and 6.2 MPa. After 100,000 fatigue cycles, compressive strength increased by 3.7%, 4.4%, and 3.0%, respectively. After 200 freeze-thaw cycles, the overall freeze-thaw durability followed the order H-GRPC > M-GRPC > L-GRPC. Microstructural analysis revealed that higher RCA quality promoted a denser matrix, a more intact interfacial transition zone, and a higher degree of geopolymerization. These findings provide guidance on selecting appropriate RCA quality for durable GRPC design.

Keywords: Recycled coarse aggregate; Geopolymer recycled pervious concrete; Mechanical property; Permeability; Durability performance

1. Introduction

With the rapid advancement of urban modernization, large quantities of construction and demolition waste are generated, leading to a series of environmental pollution issues [1,2]. Consequently, addressing resource shortages and mitigating the ecological impacts of construction waste have become critical challenges for sustainable urban development. The development and application of geopolymer recycled concrete provide an effective strategy to alleviate the excessive consumption of natural resources and to

promote the recycling of demolition debris, thereby contributing to environmental protection and circular economy objectives.

Geopolymer recycled concrete is a novel eco-friendly material synthesized by blending silicon-aluminum-rich geopolymer binders with alkali activators and recycled aggregates [3]. Typical types of geopolymer recycled concrete include fly ash-based, slag-based, and steel fiber-reinforced formulations [4–7]. Current research primarily focuses on the influence of admixtures, curing temperature, and recycled coarse aggregate (RCA) replacement ratios on the mechanical, permeability, and durability characteristics of geopolymer recycled concrete [8–13]. Guo et al. [14] reported that when the PE fiber content was 1.5%, and the slag powder content ranged from 50% to 100%, the compressive strength increased from 38 MPa to 56.1 MPa, the bridging strength reached 1.54 MPa, and the ductility improved to 6.09%, which was approximately 47 times higher than that of the fiber-free specimen. Similarly, Hamcumpai et al. [15] reported that incorporating 1% steel fibers increased the compressive strength of geopolymer recycled concrete by approximately 28% and enhanced its flexural strength by about 40%. Moreover, Moulya et al. [16] investigated the influence of RCA replacement ratios ranging from 0% to 100% and found that a replacement ratio of 70% yielded the highest compressive strength while maintaining satisfactory durability performance. Although substantial progress has been made in understanding the influence of RCA replacement ratios on the performance of geopolymer recycled concrete, the role of RCA quality in governing its mechanical behavior and long-term durability evolution remains insufficiently understood. In particular, under service conditions involving freeze-thaw action and fatigue loading, the effects of different RCA qualities on the frost resistance and fatigue behavior of geopolymer recycled concrete have not yet been systematically clarified. This knowledge gap limits the rational design and reliable application of geopolymer recycled concrete in cold-region infrastructure.

To address these issues and expand the application range of RCA, this study develops a geopolymer recycled pervious concrete (GRPC) system in which RCA is classified into three quality grades (high, medium, and low) based on apparent density. These three types of GRPC are denoted as H-GRPC, M-GRPC, and L-GRPC, respectively, and all have a uniform through-pore diameter of 1.0 mm. The effects of incorporating 40% ground granulated blast furnace slag (GBFS) and 0.3% polyvinyl alcohol (PVA) fibers on the mechanical properties, including compressive and flexural strength, and on the permeability of GRPC prepared with different RCA qualities are systematically investigated. Furthermore, X-ray diffraction (XRD) and scanning electron microscopy (SEM) are employed to elucidate the microstructural mechanisms by which RCA quality influences the material's mechanical behavior. Finally, the frost resistance and fatigue performance of GRPC are evaluated to provide a comprehensive understanding of its long-term durability and failure characteristics. The findings offer theoretical support for the sustainable application of geopolymer recycled concrete in cold-region infrastructure.

2. Materials and Methods

2.1. Materials

The coarse aggregate used in this study was RCA obtained from China Railway Urban Construction Components Co., Ltd., Changzhou, China. A single-grade aggregate with a particle size range of 4.75–9.5 mm was adopted. Three quality levels of RCA were included in the tests. These aggregates were classified into three quality grades, namely high quality, medium quality, and low quality RCA, denoted as Q1, Q2, and Q3, respectively. Their basic physical properties are presented in Table 1. The fine aggregate used in the mixtures was natural river sand with a particle size range of 0.75–4.5 mm.

The fly ash (FA) used in this study was supplied by China Railway Urban Construction Components Co., Ltd., Changzhou, China, and its main chemical composition is shown in Table 2. GBFS used in this study, which had a specific surface area of 429 m^2/kg and a moisture content of 0.5%, was provided by

Jiangsu Lvheng Environmental Technology Co., Ltd. (Changzhou, China), and its main chemical composition is presented in Table 3. The alkali activator consisted of a mixture of sodium hydroxide (NaOH) solution with a concentration of 10 mol/L and liquid sodium silicate (Na_2SiO_3) with a modulus of 2.30, a solid content of 42%, a water content of 33%, and a Baumé degree of 50. The polyvinyl alcohol (PVA) fibers were supplied by Shanghai Chemical Building Material Additives Co., Ltd. (Shanghai, China), and had a decomposition temperature of 104 °C, and a length of 12 mm.

Table 1. Physical properties of RCAs with varying quality levels.

RCA Type	Apparent Density/(kg/m^3)	Water Absorption/%	Crush Value/%
Q1	2620	4.5	11
Q2	2293	5.8	17
Q3	2242	6.5	26

Table 2. Typical chemical constituents of FA.

SiO_2/%	Al_2O_3/%	CaO/%	Fe_2O_3/%	P_2O_5/%	K_2O/%	TiO_2/%	SO_3/%
41.56	32.00	11.45	8.12	1.67	1.51	1.48	1.43

Table 3. Typical chemical constituents of GBFS.

CaO/%	SiO_2/%	Al_2O_3/%	SO_3/%	Fe_2O_3/%	MgO/%
35.79	36.32	18.63	1.73	1.08	6.35

2.2. Mix Proportion Design

As summarized in Table 4, the GRPC mixtures were proportioned with reference to JGJ 55-2011 using the volumetric method. The alkaline activator was regulated to a Na_2O:Al_2O_3 molar ratio of 0.7 and a Na_2O:H_2O mass ratio of 1:12, based on which the dosages of FA, GBFS, Na_2SiO_3, NaOH, and water were fixed at 273, 182, 173, 40, and 141 kg/m^3, respectively. To ensure comparable aggregate gradation and matrix workability among the mixtures, a constant sand ratio was maintained during mix design, thereby minimizing the influence of gradation variation on the pore structure and fresh-state behavior of GRPC. Because the apparent densities of RCA with different quality grades were different, the contents of fine aggregate and RCA were 514 kg/m^3 and 1043 kg/m^3 in L-GRPC, 534 kg/m^3 and 1083 kg/m^3 in M-GRPC, and 568 kg/m^3 and 1154 kg/m^3 in H-GRPC, respectively. In addition, the PVA fiber dosage was fixed at 3.8 kg/m^3 for all mixtures.

Table 4. Mix proportion of GRPC (kg/m^3).

Sample	Fine Aggregate	RCA	FA	GBFS	Na_2SiO_3	NaOH	PVA	Water
L-GRPC	514	1043	273	182	173	40	3.8	141
M-GRPC	534	1083	273	182	173	40	3.8	141
H-GRPC	568	1154	273	182	173	40	3.8	141

2.3. Mold Design and Specimen Preparation

The GRPC preparation process used in this study was refined based on previous research, and the overall procedure is shown in Figure 1. A custom modular mold with dimensions of 100 mm × 100 mm × 400 mm was used to prepare the GRPC specimens. As shown in Figure 2, the pore formers were arranged in a 5 × 20 array, with a center to center spacing of 20 mm and an edge distance of 10 mm, to generate uniformly distributed and interconnected longitudinal channels. Before casting, the mold was assembled, and 0.8 mm diameter steel rods were inserted as removable pore formers.

The GRPC mixture was prepared using a two-stage mixing procedure and was cast into the mold immediately after mixing, followed by vibration to ensure adequate consolidation. When the mix reached the interval between initial and final setting (approximately 5 h), the embedded steel rods were manually rotated and withdrawn to form continuous vertical channels. To prevent local instability of the pore walls, the mold was placed on its side after rod removal. Approximately 24 h after casting, the specimens were demolded, wrapped with plastic film, and subjected to thermal curing at 80 °C for 24 h, which accelerated the geopolymer hardening and gel development. Subsequently, the specimens were transferred to a standard curing environment (20 ± 2 °C, RH ≥ 95%) for 28 days, yielding the GRPC matrices required for testing.

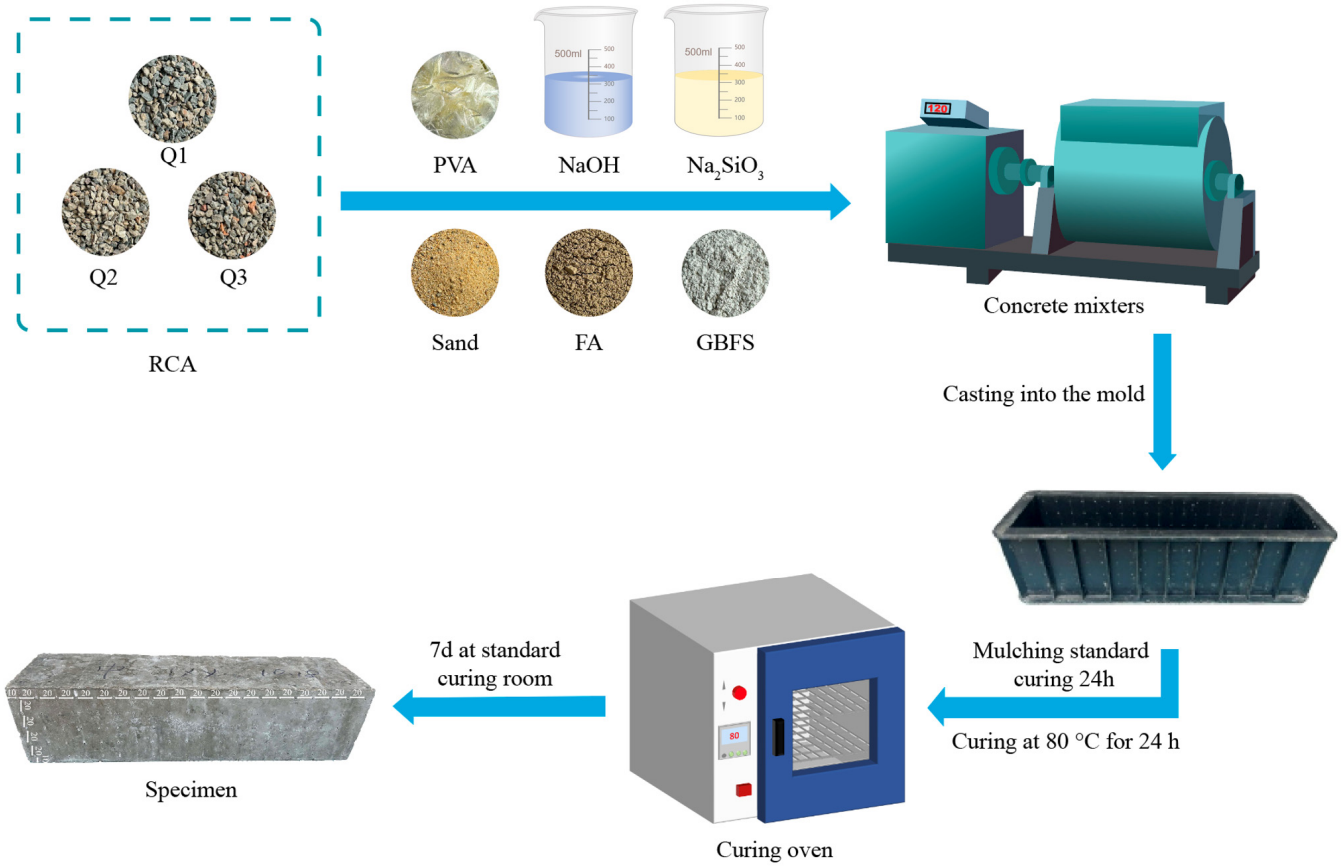

Figure 1. Process for preparing GRPC.

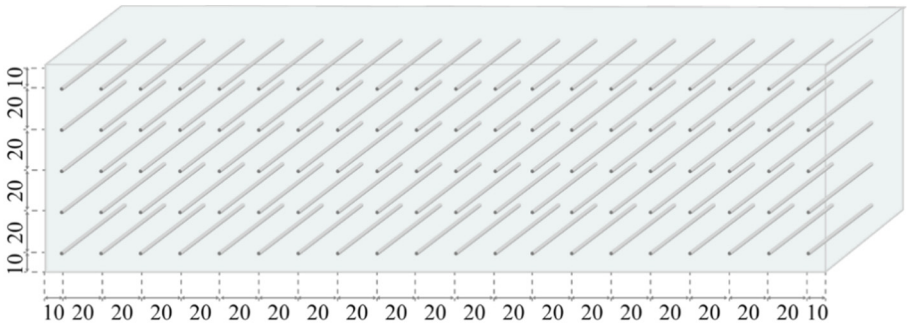

Figure 2. Mold design for GRPC specimens.

2.4. Test Methods

2.4.1. Mechanical Properties Test

According to the GB/T 50081-2019 standard [17], the compressive and flexural strengths of the GRPC specimens were determined using a WA-600C electro-hydraulic servo universal testing machine manufactured by Wuxi New Luda Instrument Equipment Co., Ltd. (Wuxi, China). Each group comprised three parallel specimens, and the strength was reported as their average value.

2.4.2. Permeability Coefficient Test

According to the CJJ/T 135-2009 standard [18], the permeability coefficient of the vertically connected pore GRPC was determined using the constant-head method. Cubic specimens with dimensions of 100 mm × 100 mm × 100 mm were used for the test. During testing, each specimen was placed in the permeability apparatus, and the gap between the specimen and the inner wall of the device was sealed with grease to prevent lateral leakage. Water was continuously supplied from the upper reservoir, and the water level was maintained at a constant head difference of 150 mm above the top surface of the specimen throughout the test. After the seepage flow became stable, the outflow water discharged from the outlet was collected for 60 s, and the permeability coefficient was calculated according to Equation (1):

$$K = \frac{QL}{AHt} \tag{1}$$

where K is the permeability coefficient (mm/s), Q is the volume of water collected within 60 s, L is the specimen thickness, A is the top surface area of the specimen, H is the constant head difference, and t is the collection time. Three parallel specimens were tested for each group, and the average value was reported. The deviation among the parallel tests was controlled within 5%.

2.4.3. Fatigue Load Test

The fatigue loading test was conducted with reference to the general requirements for concrete durability tests specified in GB/T 50082-2024 [19]. An electro-hydraulic servo fatigue testing machine was used to apply axial sinusoidal cyclic loading to the GRPC specimens, with the stress level set at 0.1–0.5 of the compressive strength and the total number of cycles fixed at 1×10^5, or until premature fatigue failure occurred. The compressive strength of the specimens was measured before and after the fatigue loading to evaluate strength degradation. Each group consisted of three parallel specimens, and the average value was reported.

2.4.4. Freeze-Thaw Resistance Test

According to the GB/T 50082-2024 standard [19], the freeze-thaw resistance of GRPC was evaluated by measuring its mass loss, compressive strength, and dynamic elastic modulus during the freeze-thaw cycles. Accelerated freeze-thaw cycling was performed in a freezing-thawing chamber with a temperature range of −14.5 to −2.5 °C, and these indicators were measured every 50 cycles. The dynamic elastic modulus was determined using a testing device operating at a frequency of 1500–3000 Hz. The mass loss rate was calculated based on Equation (2):

$$M_n = \frac{m_0 - m_n}{m_0} \tag{2}$$

where M_n is the mass loss rate after n freeze-thaw cycles, m_0 is the initial saturated mass of the specimen, m_n is the saturated surface-dry mass of the specimen after n freeze-thaw cycles, and n is the number of freeze-thaw cycles. Freeze-thaw failure was considered to occur when the compressive strength

decreased to 40% of its initial value, the mass loss rate exceeded 5%, or the relative dynamic elastic modulus (RDEM) dropped below 60%.

2.4.5. Microscopic Test

Representative samples were collected from the interior of the cured GRPC specimens for SEM and XRD analyses using the same sampling and pretreatment procedure. After drying at 105 °C for 2 h, part of the samples was cut into small pieces, sputter-coated with gold, and observed using a Zeiss SUPRA55 scanning electron microscope (Zeiss, Oberkochen, Germany) at an accelerating voltage of 15 kV and a magnification of 500×. The remaining samples were ground into powder and analyzed using a Rigaku D/Max 2500 PC X-ray diffractometer (Rigaku, Tokyo, Japan) over a 2θ range of 5°–90° at a scanning rate of 5°/min. The obtained XRD patterns were further processed using Jade 9 software for phase identification and semi-quantitative analysis.

3. Results and Discussion

3.1. Mechanical Properties

As shown in Figure 3a, the initial compressive strength of GRPC decreased with declining RCA quality, with values of 79.2 MPa, 75.3 MPa, and 60.0 MPa for H-GRPC, M-GRPC, and L-GRPC, respectively. The 24.2% reduction in L-GRPC relative to H-GRPC indicates that compressive performance was strongly dependent on RCA quality. This is mainly because high-quality RCA contains less adhered old mortar and fewer intrinsic defects, thereby providing a more stable load-bearing skeleton and a denser aggregate–matrix interface. In contrast, the higher old mortar content and poorer integrity of low-quality RCA introduced more internal defects and aggravated stress concentration under compression, leading to lower compressive strength [20–23]. The overall high strength of all mixtures was also related to the dense binding structure formed by geopolymerization and the filling effect of GBFS [24,25].

Figure 3b shows that the initial flexural strength also decreased with decreasing RCA quality, from 7.3 MPa for H-GRPC to 6.7 MPa for M-GRPC and 6.2 MPa for L-GRPC. Notably, the 15.1% reduction in flexural strength was considerably smaller than the 24.2% loss observed in compression. This difference indicates that RCA quality had a stronger influence on the integrity of the overall load-bearing skeleton than on crack resistance under bending. The superior flexural strength of H-GRPC can therefore be attributed to stronger aggregate–matrix bonding and a denser interfacial transition zone (ITZ), which effectively delay crack initiation and propagation. In contrast, the weaker interface in L-GRPC facilitated interfacial debonding and crack growth, leading to lower flexural strength [26–28]. The relatively modest reduction in flexural strength is partly attributable to the crack-bridging effect of PVA fibers and the matrix refinement induced by GBFS, which together helped restrain crack propagation under bending [29,30]. Overall, RCA quality primarily governed compressive strength through its effect on structural integrity, whereas its influence on flexural behavior was partially offset by fiber bridging and matrix densification, consistent with the microstructural characteristics discussed in Section 3.5.

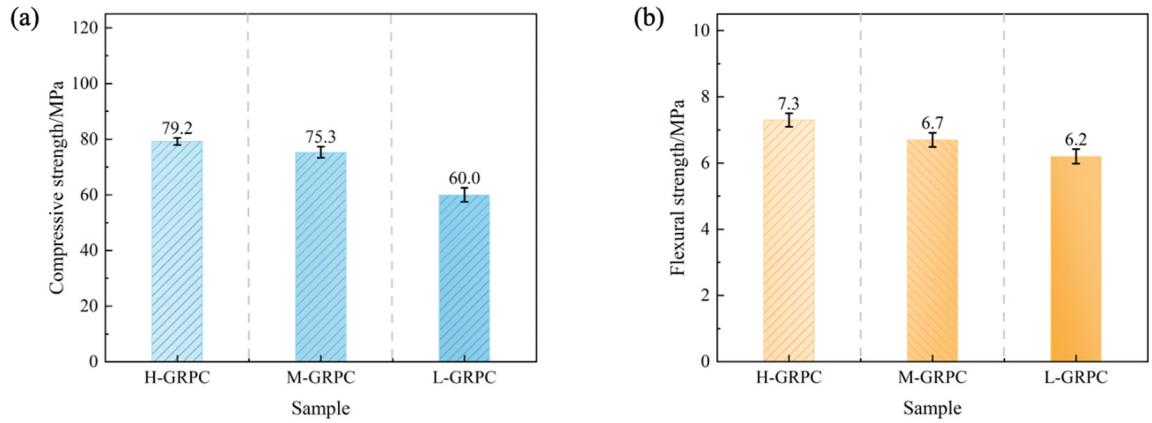

Figure 3. Strength of GRPC specimens with varying aggregate qualities: (**a**) compressive strength, (**b**) flexural strength.

3.2. Permeability Coefficient

As shown in Figure 4, the permeability coefficients of H-GRPC, M-GRPC, and L-GRPC were 0.915, 0.914, and 0.912 mm/s, respectively, with all values remaining close to 0.91 mm/s. The negligible differences among the three mixtures indicate that the permeability of GRPC was only weakly affected by RCA quality. This is mainly because the seepage behavior of GRPC was governed primarily by the preformed vertically connected pore structure rather than by the recycled aggregates themselves [31]. Since the pore diameter and arrangement were identical in all mixtures, the main seepage channels remained essentially unchanged, resulting in similar permeability coefficients. Although lower-quality RCA generally introduced more local defects, such as pores, voids, and microcracks, these features mainly contributed to local heterogeneity rather than forming continuous dominant flow paths [32,33]. Therefore, the influence of RCA quality on permeability remained secondary compared with that of the designed through-pore system. In addition, all specimens exhibited permeability coefficients markedly higher than the commonly adopted minimum requirement of 0.5 mm/s for pervious concrete, indicating that the designed GRPC possessed stable and sufficient drainage capacity. This relatively high permeability can be attributed to the vertically connected through-pore configuration, which provides more continuous flow channels and lower tortuosity than the randomly distributed voids in conventional pervious concrete, thereby reducing hydraulic resistance during water transport [34,35]. Overall, these results demonstrate that, in the present GRPC system, permeability was controlled predominantly by pore structure design, whereas variation in RCA quality had only a limited influence on overall seepage performance.

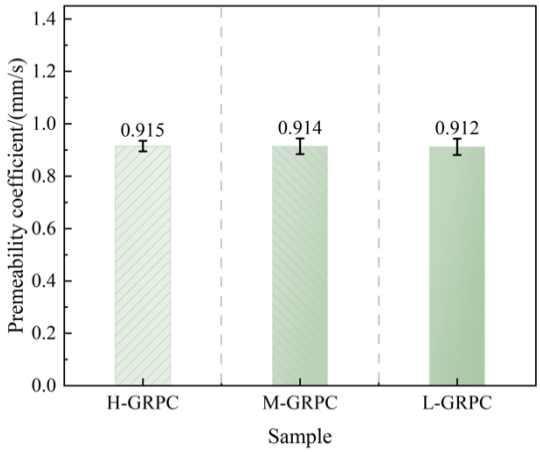

Figure 4. Permeability performance of GRPC specimens with varying aggregate qualities.

3.3. Fatigue Load Resistance

Figure 5a shows the axial load–displacement responses of the GRPC specimens under cyclic fatigue loading. Based on the flexural strength and a loading ratio of 0.1–0.5, the applied load ranges were 2.4–12 kN for H-GRPC, 2.2–11 kN for M-GRPC, and 2.0–10 kN for L-GRPC. After 100,000 cycles, the displacement ranges were 0.15–0.29 mm, 0.23–0.46 mm, and 0.20–0.45 mm for H-GRPC, M-GRPC, and L-GRPC, respectively. H-GRPC exhibited the smallest displacement range difference of 0.14 mm, which was only 56% of that of L-GRPC, indicating the strongest resistance to deformation accumulation under repeated loading. This behavior can be attributed to the more stable load-bearing skeleton and stronger aggregate–matrix interface provided by high-quality RCA, which improved local stress transfer and restrained fatigue-induced deformation [36,37]. By contrast, the larger displacement responses of M-GRPC and L-GRPC suggest a greater degree of fatigue strain development and progressive deformation accumulation during cyclic loading [38].

Figure 5b presents the compressive strengths of the three GRPC mixtures after 100,000 fatigue cycles. The compressive strengths of H-GRPC, M-GRPC, and L-GRPC were 82.1 MPa, 78.6 MPa, and 61.8 MPa, representing increases of 3.7%, 4.4%, and 3.0%, respectively, relative to their initial values. These results indicate that cyclic loading at a loading ratio of 0.1–0.5 did not cause significant structural deterioration, but instead produced a slight strengthening effect in all mixtures. This post-fatigue strength enhancement can be attributed to the combined effects of pore and microcrack closure under cyclic compression, further gel densification resulting from the continued reaction of partially reacted precursors, and improved stress transfer due to PVA fiber bridging and crack restraint [39–41]. Among the three mixtures, M-GRPC exhibited the greatest strength increase, likely because its initial structure still contained compactable pores and interfacial defects, allowing cyclic loading to induce a more pronounced compaction effect [42,43]. By contrast, H-GRPC had a denser matrix and a stronger aggregate–matrix interface before fatigue loading, leaving less room for further densification [44]. In L-GRPC, however, the weaker interfacial bonding and higher residual old mortar content limited the beneficial effects of cyclic compaction and microstructural densification, resulting in the smallest strength gain [45]. This interpretation is also consistent with the microstructural observations in Section 3.5, where H-GRPC exhibited a denser matrix and a more intact ITZ, whereas L-GRPC showed a looser interfacial structure with more defects.

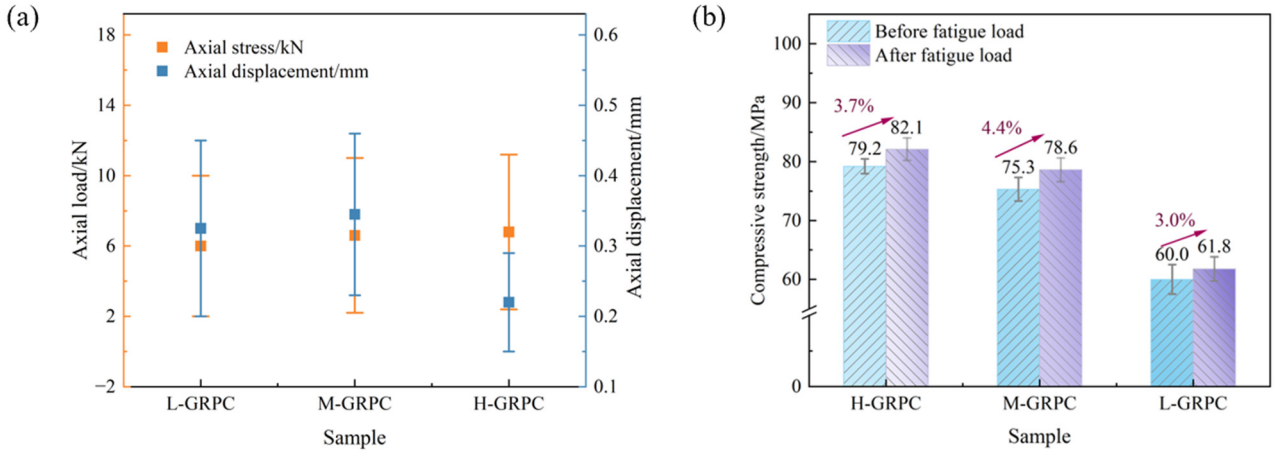

Figure 5. Mechanical response of GRPC specimens with varying qualities of RCAs: (**a**) axial load-displacement, (**b**) post-fatigue compressive strength.

3.4. Freeze-Thaw Resistance

As shown in Figure 6a, all GRPC mixtures exhibited an initial increase in mass during freeze–thaw cycling, followed by gradual stabilization or a slight decrease with further cycling. After 50 cycles, the

mass gains of H-GRPC, M-GRPC, and L-GRPC were 0.72%, 1.12%, and 1.41%, respectively, indicating that L-GRPC absorbed the largest amount of water at the early stage. This suggests that during the initial freeze–thaw period, water uptake exceeded the material loss due to surface scaling and local mortar spalling [46,47]. With increasing cycles, the mass variation of H-GRPC gradually approached zero and finally stabilized at −0.44%, whereas M-GRPC and L-GRPC exhibited larger fluctuations, ending at −1.18% and −1.60%, respectively. The more pronounced mass variation of L-GRPC is mainly associated with its less compact initial structure, weaker aggregate–matrix interface, and greater water absorption capacity, all of which increased its sensitivity to freeze–thaw action. Therefore, the larger mass fluctuation of L-GRPC should be regarded as a manifestation of higher moisture susceptibility and internal instability rather than the direct cause of freeze–thaw damage.

The evolution of RDEM in Figure 6b further reflects the accumulation of internal freeze–thaw damage in GRPC. H-GRPC and M-GRPC showed a relatively slow decrease within the first 100 cycles, followed by a more pronounced reduction thereafter, and their RDEM values finally decreased to 69.7% and 68.8%, respectively, after 200 cycles. In contrast, L-GRPC exhibited much faster early-stage deterioration, with its RDEM dropping to 73.1% after 100 cycles, indicating that internal damage developed earlier in this mixture. This behavior is mainly attributed to the lower RCA quality in L-GRPC, which facilitated water ingress and accelerated microcrack development under repeated freezing and thawing [48,49]. Although the decline rate of L-GRPC became less pronounced after 100 cycles, its RDEM remained the lowest throughout the test, suggesting that a large proportion of frost-sensitive defects had already been activated at the earlier stage. After 200 cycles, the RDEM values of all mixtures remained above the critical failure threshold of 60%, but H-GRPC maintained the highest dynamic stability, confirming its superior resistance to internal freeze–thaw deterioration.

As shown in Figure 6c, the compressive strength of all GRPC mixtures decreased markedly after 200 freeze–thaw cycles, while the residual compressive strength still followed the order of H-GRPC > M-GRPC > L-GRPC. Specifically, the residual compressive strengths of H-GRPC, M-GRPC, and L-GRPC were 48.3 MPa, 46.1 MPa, and 37.1 MPa, corresponding to strength loss rates of 39.0%, 38.8%, and 38.1%, respectively. This indicates that high-quality RCA was beneficial for maintaining a higher residual load-bearing capacity after freeze–thaw exposure, mainly because it contributed to a denser matrix and a stronger aggregate–matrix interface, thereby enhancing the stability of the internal load-bearing skeleton against freeze–thaw induced cracking and structural deterioration [50]. Although H-GRPC exhibited the highest strength loss rate, the difference was limited and should not be interpreted as inferior freeze–thaw resistance, because the strength loss ratio reflects relative degradation, whereas the residual compressive strength better represents the actual load-bearing capacity retained after cycling. By contrast, although L-GRPC showed a slightly lower strength loss rate, it exhibited the lowest residual compressive strength, indicating more severe deterioration in its overall load-bearing capacity. Therefore, the influence of RCA quality on the freeze–thaw resistance of GRPC was not simply linear, and freeze–thaw performance should be evaluated comprehensively by combining residual strength, mass variation, and RDEM evolution [51]. Overall, the larger mass fluctuation, the faster early-stage RDEM decline, and the lower residual compressive strength of L-GRPC consistently indicate that it underwent the most severe overall deterioration under freeze–thaw cycling, whereas H-GRPC exhibited the best overall freeze–thaw durability. This interpretation is also consistent with the microstructural observations in Section 3.5, where H-GRPC exhibited a denser matrix and more intact interfacial bonding, whereas L-GRPC showed a looser ITZ structure with more pores and cracks.

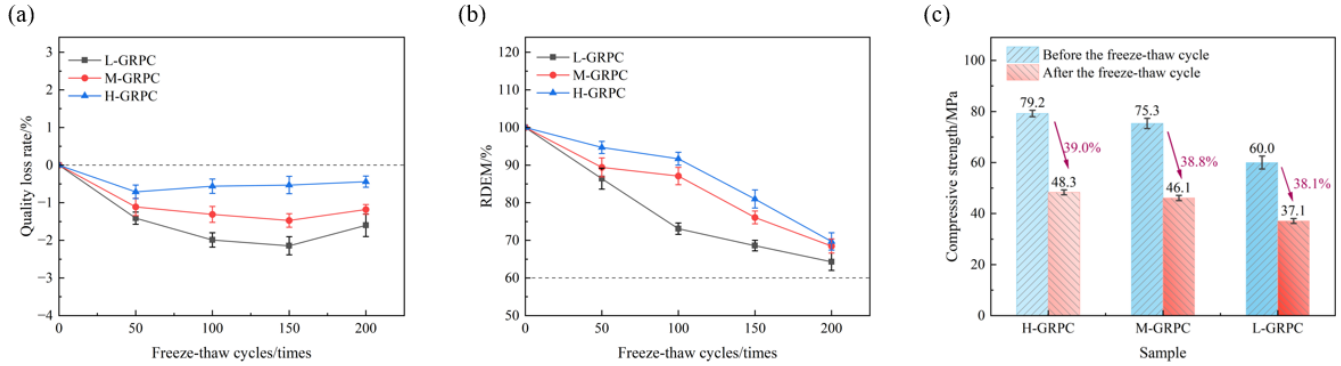

Figure 6. Freeze-thaw durability of GRPC specimens: (**a**) mass change, (**b**) RDEM, (**c**) compressive strength after freeze-thaw cycles.

3.5. Microstructural Analysis

As shown in Figure 7, the SEM micrographs revealed clear microstructural differences among the GRPC mixtures prepared with different RCA qualities. All specimens contained internal pores and unreacted spherical fly ash particles within the mortar matrix, although their abundance and distribution varied substantially. H-GRPC exhibited the densest microstructure, with fewer visible pores and microcracks, and the PVA fibers were well embedded in the geopolymer matrix, indicating a more integrated internal structure. This is likely associated with the lower amount of adhered old mortar in high-quality RCA, which reduced internal defects and provided more favorable conditions for matrix formation and interfacial bonding. In contrast, M-GRPC showed a relatively wider ITZ accompanied by several intersecting microcracks, suggesting a moderate reduction in interfacial compactness. L-GRPC exhibited the loosest ITZ structure, with more extensive cracks and voids distributed around the aggregate–matrix interface, reflecting weaker interfacial bonding and a more defective microstructure. These microstructural differences indicate that the decline in RCA quality progressively weakened the compactness of the matrix and the integrity of the ITZ, which is consistent with the lower initial mechanical performance, greater deformation accumulation under fatigue loading, and higher susceptibility to freeze–thaw deterioration observed in L-GRPC.

As shown in Figure 8, clear diffraction peaks of Quartz, Calcite, and Gismondite were identified in all GRPC specimens, indicating that the main crystalline phases consisted of unreacted quartz, carbonate-related products, and geopolymerization-related crystalline phases. To evaluate the relative phase variations under different RCA qualities, semi quantitative analysis was performed on the XRD patterns using Jade software. Two representative characteristic peaks without obvious overlap were selected for each phase, and their average peak area was adopted as the representative intensity after local baseline subtraction and normalization according to Equation (3):

$$P_i = \frac{\bar{A}_i}{\bar{A}_Q + \bar{A}_C + \bar{A}_Z} \tag{3}$$

where P_i is the relative content of phase i, and $\bar{A}_i$ is the average area of the two characteristic peaks of that phase. According to the standard phase reference cards from the international Centre for Diffraction Data (ICDD) PDF database [52], the selected peaks were located at 2θ = 26.66° and 50.14° for Quartz, 2θ = 29.42° and 39.48° for Calcite, and 2θ = 16.42° and 20.86° for Gismondite. The corresponding semi quantitative results are listed in Table 5.

According to Table 5, Quartz remained the dominant crystalline phase in all specimens, with relative contents of 72.77%, 76.49%, and 78.30% in H-GRPC, M-GRPC, and L-GRPC, respectively. Its gradual increase with decreasing RCA quality further suggests that the lower quality RCA systems retained a relatively higher proportion of unreacted crystalline phases. In contrast, the Gismondite content decreased

from 18.68% in H-GRPC to 14.27% in M-GRPC, and then to 8.24% in L-GRPC, indicating a progressive reduction in the geopolymerization degree and in reaction product formation as RCA quality declined. Meanwhile, Calcite showed the opposite trend, increasing from 8.55% to 9.23% and then to 13.46%. This increase is mainly associated with the higher amount of adhered old mortar and carbonate containing components in the low-quality RCA, while the looser and more defective internal structure may also have promoted subsequent carbonation [53]. Overall, the decrease in Gismondite, together with the increase in Quartz and Calcite, indicates that reduced RCA quality weakened the geopolymerization reaction and increased the proportions of unreacted phases and carbonation products. This interpretation agrees well with the SEM observations, where H-GRPC showed a denser and more intact microstructure, whereas L-GRPC exhibited more pores, cracks, and a looser ITZ structure.

Table 5. Semi quantitative results of major crystalline phases in different GRPC specimens based on the dual peak method.

Sample	Quartz (%)	Calcite (%)	Gismondite (%)
L-GRPC	78.30	13.46	8.24
M-GRPC	76.49	9.23	14.27
H-GRPC	72.77	8.55	18.68

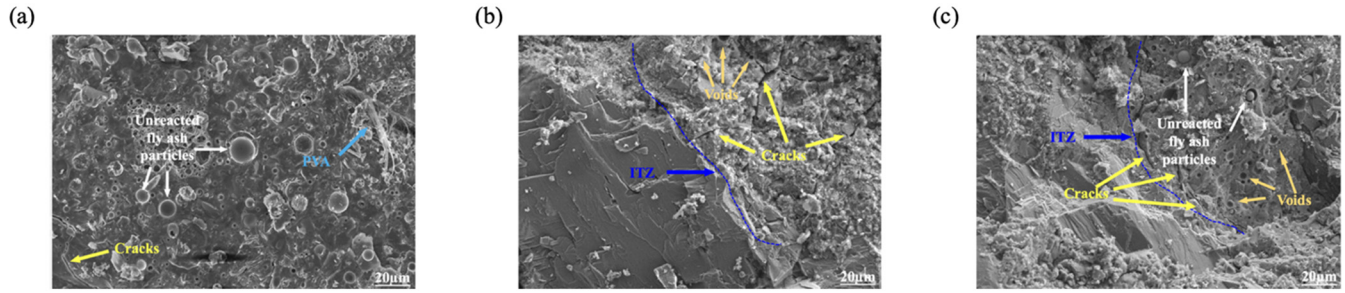

Figure 7. Microstructural SEM observations of different GRPC specimens (magnification: 500×): (**a**) H-GRPC, (**b**) M-GRPC, (**c**) L-GRPC.

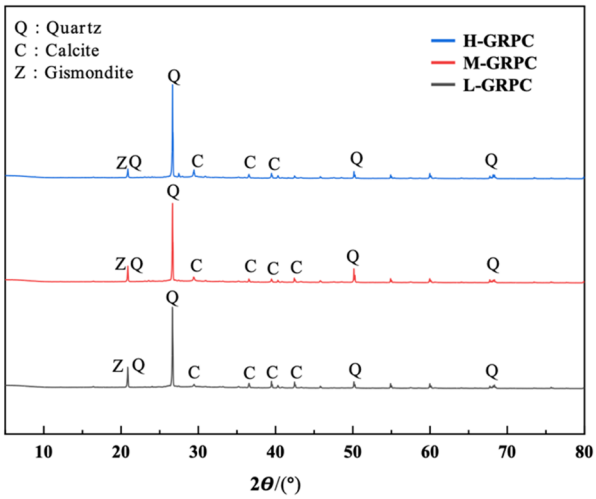

Figure 8. XRD results of GRPC specimens with varying aggregate qualities.

In summary, H-GRPC exhibited the best overall performance in terms of strength, fatigue resistance, and freeze-thaw durability, followed by M-GRPC, while L-GRPC showed the weakest behavior. These differences were mainly governed by the quality dependent variations in matrix compactness, ITZ integrity, and geopolymerization degree. High-quality RCA, with less adhered old mortar and fewer inherent defects, contributed to a denser matrix and a stronger aggregate-matrix interface, thereby improving stress transfer

and maintaining higher mechanical stability under loading [54]. In contrast, low-quality RCA introduced more pores, voids, residual old mortar, and microcracks into the system, which promoted interfacial debonding and crack propagation, leading to lower strength and poorer durability [55]. By comparison, the permeability coefficients of the three mixtures remained similar because the seepage behavior of GRPC was controlled mainly by the predesigned vertically connected through-pore structure. Under cyclic fatigue loading, all mixtures showed a slight increase in compressive strength, which can be attributed to local crack closure, continued geopolymerization, and the crack-bridging effect of PVA fibers [56]. However, the strengthening effect was less pronounced in L-GRPC because its weaker interface and greater defect content limited the beneficial effects of cyclic compaction. During freeze-thaw cycling, the larger amount of residual old mortar, together with the presence of more pores and microcracks in L-GRPC, facilitated water ingress and crack development, resulting in more severe internal deterioration and lower residual performance [57,58].

4. Conclusions

This study systematically investigated the influence of RCA quality on the mechanical and durability performance of GRPC through macroscopic and microscopic characterization. The main conclusions are as follows:

(1) The quality of RCA significantly affected the mechanical performance of GRPC. Both compressive and flexural strengths increased with increasing RCA quality, with H-GRPC exhibiting the highest initial compressive strength of 79.2 MPa and flexural strength of 7.3 MPa. The superior mechanical behavior of H-GRPC was mainly associated with its denser internal structure, lower defect content, and stronger aggregate–matrix interface, whereas the higher adhered mortar content and intrinsic defects in low-quality RCA weakened the load-bearing skeleton and promoted stress concentration.

(2) The permeability coefficient of GRPC was only marginally affected by RCA quality. The permeability coefficients of H-GRPC, M-GRPC, and L-GRPC all remained around 0.91 mm/s, indicating negligible differences among the three mixtures. This suggests that the permeability of the present GRPC system was mainly governed by the predesigned vertically connected through-pore structure, whereas defects introduced by low-quality RCA mainly increased local microstructural heterogeneity without significantly altering the dominant seepage channels.

(3) Under cyclic fatigue loading, H-GRPC exhibited the best resistance to deformation accumulation, as reflected by the smallest displacement range difference of 0.14 mm. After 100,000 fatigue cycles, all mixtures showed slight increases in compressive strength, with strength gains of 3.7%, 4.4%, and 3.0% for H-GRPC, M-GRPC, and L-GRPC, respectively. These results indicate that the applied fatigue loading conditions did not induce apparent structural deterioration but instead produced a mild compaction and strengthening effect in the GRPC system.

(4) Freeze-thaw cycling caused significant deterioration in all GRPC mixtures, but the overall freeze-thaw durability still followed the order H-GRPC > M-GRPC > L-GRPC when evaluated comprehensively using mass variation, relative dynamic elastic modulus, and residual compressive strength. After 200 cycles, H-GRPC showed the smallest mass fluctuation and retained the highest residual compressive strength, whereas L-GRPC exhibited larger mass variation, faster early-stage RDEM decline, and the lowest residual compressive strength, indicating more severe internal deterioration.

(5) Microstructural analyses confirmed that differences in matrix compactness, ITZ integrity, and the degree of geopolymerization fundamentally governed the effect of RCA quality on GRPC performance. High-quality RCA promoted a denser matrix, a stronger aggregate–matrix interface, and a higher proportion of geopolymerization-related phases, thereby improving stress transfer efficiency and resistance to fatigue and freeze-thaw damage. In contrast, low-quality RCA introduced more residual

mortar, pores, and cracks, resulting in a looser ITZ, a lower geopolymerization degree, and inferior overall mechanical and durability performance.

Statement of the Use of Generative AI and AI-Assisted Technologies in the Writing Process

During the preparation of this manuscript, the authors used DeepL in order to assist with translation, improve English language expression, and enhance readability. After using this tool, the authors reviewed and edited the content as needed and take full responsibility for the content of the published article.

Acknowledgments

The authors sincerely thank China Railway Urban Construction Components Co., Ltd. (Changzhou, China) for supplying the recycled coarse aggregates and fly ash used in this study. Appreciation is also extended to Jiangsu Lvheng Environmental Technology Co., Ltd. (Changzhou, China) for providing the ground granulated blast furnace slag. The technical assistance from the laboratory staff at Changzhou University is gratefully acknowledged.

Author Contributions

Methodology, Y.S.; Formal Analysis, Y.S., X.L., H.L., M.Z., Y.S. and F.D.; Writing—Original Draft Preparation, Y.S. and M.Z.; Writing—Review & Editing, Y.S., X.L., H.L., P.Z., Y.S. and F.D.; Project Administration, P.Z.; Funding Acquisition, M.Z.

Ethics Statement

Not applicable.

Informed Consent Statement

Not applicable.

Data Availability Statement

Data will be made available on request.

Funding

This research was supported by the National Natural Science Foundation of China (No. 42202034) and the Open Fund of the Key Laboratory of Solid Waste Treatment and Resource Reuse, Ministry of Education (No. 22kfgk03).

Declaration of Competing Interest

The authors declare that they have no known competing financial interests or personal relationships that could have appeared to influence the work reported in this paper.

References

1. Wang Q, Chen L, Hu R, Ren Z, He Y, Liu D, et al. An empirical study on waste generation rates at different stages of construction projects in China. *Waste Manag. Res.* **2020**, *38*, 433–443. DOI:10.1177/0734242X19886635
2. Bakshan A, Srour I, Chehab G, El-Fadel M. A field based methodology for estimating waste generation rates at various stages of construction projects. *Resour. Conserv. Recycl.* **2015**, *100*, 70–80. DOI:10.1016/j.resconrec.2015.04.002
3. Zhang P, Sun X, Wang F, Wang J. Mechanical properties and durability of geopolymer recycled aggregate concrete: A review. *Polymers* **2023**, *15*, 615. DOI:10.3390/polym15030615
4. Nuaklong P, Sata V, Chindaprasirt P. Influence of recycled aggregate on fly ash geopolymer concrete properties. *J. Clean.*

Prod. **2016**, *112*, 2300–2307. DOI:10.1016/j.jclepro.2015.10.109
5. Zhang D, Zhu T, Yang Q, Vandeginste V, Li J. Influence of ground granulated blast furnace slag on recycled concrete powder-based geopolymer cured at ambient temperature: Rheology, mechanical properties, reaction kinetics and air-void characteristics. *Constr. Build. Mater.* **2024**, *438*, 137190. DOI:10.1016/j.conbuildmat.2024.137190
6. Wen Y, Liu X, Sun G, Shen W. Mechanical properties and stress-strain relationship of steel fiber reinforced geopolymer recycled concrete. *Structures* **2025**, *75*, 108697. DOI:10.1016/j.istruc.2025.108697
7. Ahıskalı A, Ahıskalı M, Bayraktar OY, Kaplan G, Assaad J. Mechanical and durability properties of polymer fiber reinforced one-part foam geopolymer concrete: A sustainable strategy for the recycling of waste steel slag aggregate and fly ash. *Constr. Build. Mater.* **2024**, *440*, 137492. DOI:10.1016/j.conbuildmat.2024.137492
8. Wang J, Xie J, Wang C, Zhao J, Liu F, Fang C. Study on the optimum initial curing condition for fly ash and GGBS based geopolymer recycled aggregate concrete. *Constr. Build. Mater.* **2020**, *247*, 118540. DOI:10.1016/j.conbuildmat.2020.118540
9. Chen J, Duan J, Zhu Q, Jin W, Lu C, Lv M, et al. High temperature resistance of slag/fly ash-based geopolymer concrete with fully recycled coarse aggregate. *Constr. Build. Mater.* **2025**, *482*, 141587. DOI:10.1016/j.conbuildmat.2025.141587
10. Mahmoodi O, Siad H, Lachemi M, Dadsetan S, Şahmaran M. Extensive rheological evaluation of geopolymer mortars incorporating maximum amounts of recycled concrete as precursors and aggregates. *Constr. Build. Mater.* **2023**, *390*, 131801. DOI:10.1016/j.conbuildmat.2023.131801
11. Kumar VV. Study on fresh and mechanical properties for different grades of geopolymer concrete with recycled coarse aggregate. *Mater. Today Proc.* **2022**, *60*, 708–714. DOI:10.1016/j.matpr.2022.02.326
12. Singh PK, Rajhans P. Effect of surface treatment and mixing approach on the durability performance of recycled aggregate geopolymer concrete against aggressive environment. *J. Build. Eng.* **2025**, *101*, 111867. DOI:10.1016/j.jobe.2025.111867
13. Saloni, Parveen, Lim YY, Pham TM. Effective utilisation of ultrafine slag to improve mechanical and durability properties of recycled aggregates geopolymer concrete. *Clean. Eng. Technol.* **2021**, *5*, 100330. DOI:10.1016/j.clet.2021.100330
14. Guo J, Liu Q, Pan H, Sun Y, Guo B. Investigation on the workability, mechanical properties and carbon emission performance of fiber-reinforced geopolymer recycled concrete (FRGRC). *Constr. Build. Mater.* **2025**, *474*, 141004. DOI:10.1016/j.conbuildmat.2025.141004
15. Hamcumpai K, Nuaklong P, Chindasiriphan P, Jongvivatsakul P, Likitlersuang S, Di Sarno L, et al. Enhancing high-strength geopolymer concrete with recycled granite aggregate using sugarcane bagasse ash and steel fibers. *Constr. Build. Mater.* **2025**, *493*, 143096. DOI:10.1016/j.conbuildmat.2025.143096
16. Moulya HV, Chandrashekhar A. Experimental investigation of effect of recycled coarse aggregate properties on the mechanical and durability characteristics of geopolymer concrete. *Mater. Today Proc.* **2022**, *59*, 1700–1707. DOI:10.1016/j.matpr.2022.03.403
17. *GB/T 50081-2019*; Standard for Test Methods of Mechanical Properties of Ordinary Concrete. Standardization Administration of China: Beijing, China, 2019.
18. *CJJ/T 135-2009*; Technical Specification for Recycled Aggregate Concrete. Ministry of Housing and Urban-Rural Development of the People's Republic of China: Beijing, China, 2009.
19. *GB/T 50082-2024*; Standard for Test Methods of Long-Term Performance and Durability of Ordinary Concrete. Standardization Administration of China: Beijing, China, 2024.
20. Zheng R, Zhang F, Wang D, Wang M, Wang J. Basic mechanical properties of geopolymer recycled concrete with iron ore tailings sand. *J. Build. Eng.* **2025**, *114*, 114331. DOI:10.1016/j.jobe.2025.114331
21. Yuan S, Wan H, Gao L, Teng J, Shi N, Liu Z, et al. Bio-mineralization strengthened ITZ in solid waste-based recycled concrete: Enhanced mechanical properties and sulfate attack resistance. *Structures* **2025**, *80*, 109957. DOI:10.1016/j.istruc.2025.109957
22. Guo M, Grondin F, Loukili A. Numerical analysis of the failure of recycled aggregate concrete by considering the random composition of old attached mortar. *J. Build. Eng.* **2020**, *28*, 101040. DOI:10.1016/j.jobe.2019.101040
23. Duan ZH, Poon CS. Properties of recycled aggregate concrete made with recycled aggregates with different amounts of old adhered mortars. *Mater. Des.* **2014**, *58*, 19–29. DOI:10.1016/j.matdes.2014.01.044
24. Diaz Caselles L, Balsamo B, Benavent V, Trincal V, Lahalle H, Patapy C, et al. Behavior of calcined clay based geopolymers under sulfuric acid attack: Meta-illite and metakaolin. *Constr. Build. Mater.* **2023**, *363*, 129889. DOI:10.1016/j.conbuildmat.2022.129889
25. Chen X, Guo Y, Ding S, Zhang H, Xia F, Wang J, et al. Utilization of red mud in geopolymer-based pervious concrete with function of adsorption of heavy metal ions. *J. Clean. Prod.* **2019**, *207*, 789–800. DOI:10.1016/j.jclepro.2018.09.263
26. Zhu X, Zhu P, Liu H, Yan X, Chen C. Recyclability potential of multi-generation carbonated recycled aggregate concrete under coupling action of high stress and freeze-thaw cycles. *J. Build. Eng.* **2025**, *114*, 114333.

DOI:10.1016/j.jobe.2025.114333
27. Wang X, Yang J, Wu Y, Zhu P, Yan X, Liu H. Tailoring high ductility cementitious composite incorporating recycled fine aggregate based on shrinkage and mechanical properties. *J. Build. Eng.* **2024**, *93*, 109868. DOI:10.1016/j.jobe.2024.109868
28. Liu H, Liu X, Wang X, Zhu P, Yang L, Yan X. The impact of original aggregate and attached mortar types of recycled aggregates on the sulfuric acid resistance of geopolymer recycled concrete. *J. Build. Eng.* **2024**, *82*, 108273. DOI:10.1016/j.jobe.2023.108273
29. Tan J, Cai J, Li X, Pan J, Li J. Development of eco-friendly geopolymers with ground mixed recycled aggregates and slag. *J. Clean. Prod.* **2020**, *256*, 120369. DOI:10.1016/j.jclepro.2020.120369
30. Zhang P, Gao Z, Wang J, Wang K. Numerical modeling of rebar-matrix bond behaviors of nano-SiO_2 and PVA fiber reinforced geopolymer composites. *Ceram. Int.* **2021**, *47*, 11727–11737. DOI:10.1016/j.ceramint.2021.01.012
31. Aliabdo AA, Abd Elmoaty AEM, Fawzy AM. Experimental investigation on permeability indices and strength of modified pervious concrete with recycled concrete aggregate. *Constr. Build. Mater.* **2018**, *193*, 105–127. DOI:10.1016/j.conbuildmat.2018.10.182
32. Gao Z, Lei D, Chen H, He J, Kong E, Xu Y. Characterization of interfacial transition zone of fly ash concrete with different coarse-aggregates by optical microscopy and digital image correlation coupled method. *Mater. Today Commun.* **2023**, *34*, 105099. DOI:10.1016/j.mtcomm.2022.105099
33. Lian S, Ruan S, Zhan S, Unluer C, Meng T, Qian K. Unlocking the role of pores in chloride permeability of recycled concrete: A multiscale and a statistical investigation. *Cem. Concr. Compos.* **2022**, *125*, 104320. DOI:10.1016/j.cemconcomp.2021.104320
34. Debnath B, Sarkar PP. Permeability prediction and pore structure feature of pervious concrete using brick as aggregate. *Constr. Build. Mater.* **2019**, *213*, 643–651. DOI:10.1016/j.conbuildmat.2019.04.099
35. Yu F, Sun D, Hu M, Wang J. Study on the pores characteristics and permeability simulation of pervious concrete based on 2D/3D CT images. *Constr. Build. Mater.* **2019**, *200*, 687–702. DOI:10.1016/j.conbuildmat.2018.12.135
36. Andal J, Shehata M, Zacarias P. Properties of concrete containing recycled concrete aggregate of preserved quality. *Constr. Build. Mater.* **2016**, *125*, 842–855. DOI:10.1016/j.conbuildmat.2016.08.110
37. Gan Y, Zhang H, Liang M, Zhang Y, Schlangen E, van Breugel K, et al. Flexural strength and fatigue properties of interfacial transition zone at the microscale. *Cem. Concr. Compos.* **2022**, *133*, 104717. DOI:10.1016/j.cemconcomp.2022.104717
38. Xiao J, Li H, Yang Z. Fatigue behavior of recycled aggregate concrete under compression and bending cyclic loadings. *Constr. Build. Mater.* **2013**, *38*, 681–688. DOI:10.1016/j.conbuildmat.2012.09.024
39. Becks H, Classen M. Influence of coarse aggregates on the fatigue behavior of high-strength concrete under mode II loading. *Constr. Build. Mater.* **2025**, *491*, 142565. DOI:10.1016/j.conbuildmat.2025.142565
40. Luo Y, Klima KM, Brouwers HJH, Yu Q. Effects of ladle slag on Class F fly ash geopolymer: Reaction mechanism and high temperature behavior. *Cem. Concr. Compos.* **2022**, *129*, 104468. DOI:10.1016/j.cemconcomp.2022.104468
41. Ling Y, Zhang P, Wang J, Chen Y. Effect of PVA fiber on mechanical properties of cementitious composite with and without nano-SiO_2. *Constr. Build. Mater.* **2019**, *229*, 117068. DOI:10.1016/j.conbuildmat.2019.117068
42. Ren Q, Pacheco J, de Brito J, Hu J. Analysis of the influence of the attached mortar's geometry on the mechanical behaviour of recycled aggregate concrete through mesoscale modelling. *Eng. Fract. Mech.* **2024**, *297*, 109876. DOI:10.1016/j.engfracmech.2024.109876
43. Sainz-Aja J, Carrascal I, Polanco JA, Thomas C. Fatigue failure micromechanisms in recycled aggregate mortar by μCT analysis. *J. Build. Eng.* **2020**, *28*, 101027. DOI:10.1016/j.jobe.2019.101027
44. Xu F, Kong F, Xiong Q, Li Y, Zhu J, Sun T, et al. Internal interfacial interaction analysis of geopolymer-recycled aggregate pervious concrete based on a infiltration model. *Constr. Build. Mater.* **2022**, *333*, 127417. DOI:10.1016/j.conbuildmat.2022.127417
45. Yang W, Liu H, Zhu P, Zhu X, Liu X, Yan X. Effect of recycled coarse aggregate quality on the interfacial property and sulfuric acid resistance of geopolymer concrete at different acidity levels. *Constr. Build. Mater.* **2023**, *375*, 130919. DOI:10.1016/j.conbuildmat.2023.130919
46. Wei D, Zhu P, Yan X, Liu H, Chen C, Wang Z. Potential evaluation of waste recycled aggregate concrete for structural concrete aggregate from freeze-thaw environment. *Constr. Build. Mater.* **2022**, *321*, 126291. DOI:10.1016/j.conbuildmat.2021.126291
47. Luan H, Wu J, Pan J. Saline water absorption behavior and critical saturation degree of recycled aggregate concrete during freeze-thaw cycles. *Constr. Build. Mater.* **2020**, *258*, 119640. DOI:10.1016/j.conbuildmat.2020.119640
48. Cai S, Lin J, Fan K, Chen Y, Wang Z. Study on the bonding performance between basalt textile and concrete under freeze-thaw cycles. *Eng. Fail. Anal.* **2023**, *146*, 107095. DOI:10.1016/j.engfailanal.2023.107095
49. Zhao R, Yuan Y, Cheng Z, Wen T, Li J, Li F, et al. Freeze-thaw resistance of class F fly ash-based geopolymer concrete.

Constr. Build. Mater. **2019**, *222*, 474–483. DOI:10.1016/j.conbuildmat.2019.06.166
50. Zhang H, Zheng R, Wu G, Yao Y, Bao J. Improving the frost resistance of recycled aggregate concrete: A comprehensive review. *J. Build. Eng.* **2025**, *114*, 114249. DOI:10.1016/j.jobe.2025.114249
51. Liu H, Dai X, Zhu P, Wang X, Zong M, Feng J. Acid rain resistance of geopolymer recycled pervious concrete featuring top-bottom interconnected pores under freeze-thaw cycles and fatigue loads. *J. Build. Eng.* **2024**, *96*, 110356. DOI:10.1016/j.jobe.2024.110356
52. International Centre for Diffraction Data (ICDD). *PDF-4+ Database*; International Centre for Diffraction Data (ICDD): Newtown Square, PA, USA, 2023.
53. Shuvo AK, Sarker PK, Shaikh FUA. Efficacy of various accelerated carbonation techniques to improve recycled concrete aggregates: A comprehensive review. *J. Build. Eng.* **2024**, *95*, 110257. DOI:10.1016/j.jobe.2024.110257
54. Kim J. Influence of quality of recycled aggregates on the mechanical properties of recycled aggregate concretes: An overview. *Constr. Build. Mater.* **2022**, *328*, 127071. DOI:10.1016/j.conbuildmat.2022.127071
55. Chakraborty S, Subramaniam KVL. Evaluation of cracking and cohesive fracture response in recycled aggregate concrete. *Mater. Struct.* **2023**, *56*, 130. DOI:10.1617/s11527-023-02193-x
56. De La Rosa Á, Ortega JJ, Ruiz G, García Calvo JL, Rubiano Sánchez FJ, Castillo Á. Autogenous self-healing induced by compressive fatigue in self-compacting steel-fiber reinforced concrete. *Cem. Concr. Res.* **2023**, *173*, 107278. DOI:10.1016/j.cemconres.2023.107278
57. Amorim Júnior NS, Silva GAO, Ribeiro DV. Effects of the incorporation of recycled aggregate in the durability of the concrete submitted to freeze-thaw cycles. *Constr. Build. Mater.* **2018**, *161*, 723–730. DOI:10.1016/j.conbuildmat.2017.12.076
58. Bogas JA, De Brito J, Ramos D. Freeze–thaw resistance of concrete produced with fine recycled concrete aggregates. *J. Clean. Prod.* **2016**, *115*, 294–306. DOI:10.1016/j.jclepro.2015.12.065